Comparison of the Structure of Polyelectrolyte Multilayer Films Exhibiting a Linear and an Exponential Growth Regime: An in Situ Atomic Force Microscopy Study

Ph. Lavalle,*,† C. Gergely,† F. J. G. Cuisinier,† G. Decher,‡,§ P. Schaaf,‡,⊥ J. C. Voegel,† and C. Picart†,⊥

INSERM Unité 424, Fédération de Recherches "Odontologie", Université Louis Pasteur, 11 rue Humann, F-67085 Strasbourg Cedex, France; Institut Charles Sadron (CNRS UPR 22), 6 rue Boussingault, F-67083 Strasbourg Cedex, France; Université Louis Pasteur, Faculté de Chimie, 1 rue Blaise Pascal, F-67008 Strasbourg Cedex, France; and Ecole Européenne de Chimie, Polymères et Matériaux de Strasbourg, 25, rue Becquerel, F-67087 Strasbourg Cedex 2, France

Received November 13, 2001; Revised Manuscript Received March 13, 2002

ABSTRACT: We report here on the structural characterization of polyelectrolytes multilayer films formed by poly(L-glutamic acid) and poly(L-lysine) (PGA/PLL). The growth of this system is compared to that of poly(styrenesulfonate)/poly(allylamine hydrochloride) (PSS/PAH) multilayers by means of in situ atomic force microscopy (AFM) and by optical waveguide lightmode spectroscopy (OWLS). In contrary to the $(PSS/PAH)_i$ films that are growing linearly with the number of deposited layer pairs *i*, optical data evidenced that the $(PGA/PLL)_i$ films are characterized by an exponential growth. The analysis of the structure of the $(PSS/PAH)_i$ films reveals a smooth featureless surface covered by small globules. On the other hand, $(PGA/PLL)_i$ films form extended structures that appear with a vermiculate pattern. We propose a new growth mechanism based on polyelectrolyte diffusion in and out of the film coupled to the formation of polyanion/polycation complexes at the surface of the film in order to explain the whole results.

I. Introduction

The alternate immersion of a charged surface in a polyanion and a polycation solution leads usually to the formation of films known as polyelectrolyte multilayers.[1,2] These polyanion/polycation structures are not neutral, but a charge overcompensation appears on the surface; this constitutes the buildup motor of the polyelectrolyte multilayer films.[3] The first films that were explored were built with highly charged polyelectrolytes, such as poly(styrenesulfonate) and poly(allylamine hydrochloride), afterward denoted (PSS/PAH).[4] These films exhibited remarkable and fascinating properties: the film thickness and the deposited amount of polyelectrolytes increased typically linearly with the number of deposited layer pairs.[5−7] They present a layered structure, each polyelectrolyte layer interpenetrating with some of the closest neighboring ones.[2,8,9] However, recent experimental results seem to indicate that the ideal picture of a linearly growing stratified smooth film does not constitute the only possible buildup mechanism. Parameters such as the chemical nature of the polymer pair, the nature and concentration of salt added to solutions used for deposition and/or rinsing, and others have a strong influence on the nature of the polyion complex formed. Experimental evidence supports the idea that, by increasing the salt concentration for a given system, the film thickness and the adsorbed amount of polyelectrolytes can increase more rapidly than linearly with the number of deposited layer pairs.[10−13] This change from a linear to a superlinear growth regime was suggested for the PSS/PAH[10] and for the poly(diallyldimethylammonium chloride)/poly(styrenesulfonate) (PDDA/PSS)[12] film architectures. Other systems composed of glycosaminoglycans and poly(L-lysine) also exhibit such a superlinear growth regime.[14−17]

Recently, McAloney et al.[12] followed the buildup process of PDDA/PSS multilayers by AFM and studied the film structure at different ionic strength of the building polyelectrolyte solutions. Their images revealed that the film was featureless and slightly granular at low ionic strength when the film growth can be described as being linear. For salt concentration higher than 0.3 M the film growth changes to overshooting mode, and a vermiculate surface pattern associated with an increase of the film roughness was observed. It is thus tempting to associate a linear growth regime to a flat smooth film and a superlinear regime to a more rough and "heterogeneous" film topography. Unfortunately, all these studies were performed by rinsing the films in pure water after each polyelectrolyte deposition step during their buildup process and by imaging the film after the multilayer had been dried. It is known that pH and ionic strength jumps applied during or after the film construction can anneal surface roughness[18] but also lead to more dramatic structural rearrangements such as inducing porosity in the multilayer structure.[19,20] Moreover, there exist indications that the film structure is also altered by the drying process.[21]

The goal of the present article is to provide further information on the mechanisms that lead either to a linear or to a superlinear growth regime and in particular to verify whether this superlinear growth regime is always associate with increased surface roughness. Therefore, we investigate the buildup of poly(L-glutamic acid)/poly(L-lysine) (PGA/PLL) multilayer films grown under superlinear conditions by means of in situ AFM and by optical waveguide lightmode spectroscopy

† INSERM.
‡ Institut Charles Sadron.
§ Université Louis Pasteur.
⊥ Polymères et Matériaux de Strasbourg.
* Corresponding author.

10.1021/ma0119833 CCC: $22.00
Published on Web 04/27/2002

(OWLS), which yields information on both the film thickness and the amount of adsorbed polyelectrolyte. These results will be compared with the more widely studied PSS/PAH system that typically shows linear growth. Great care was taken to perform all the experiments and in particular the AFM observations under conditions that minimize any film restructuration. Toward this end, the films will be constructed and imaged in buffer solutions over the whole buildup process. The film construction will be followed up to the 10th layer pairs. We will propose a growth mechanism based on polyelectrolyte diffusion in and out the film during the buildup process, which allows to explain both the exponential growth and the observed topography of the PGA/PLL multilayers. Moreover, this mechanism also explains results obtained previously for films composed of poly(L-lysine) and hyaluronic acid (PLL/HA) that also exhibit superlinear growth.[17]

II. Materials and Methods

Polyelectrolyte Solutions. Poly(sodium 4-styrenesulfonate) (PSS, MW = 7.0×10^4 Da), poly(allylamine hydrochloride) (PAH, MW = 7.0×10^4 Da), poly(L-lysine) (PLL, MW = 3.26×10^4 Da), and poly(L-glutamic acid) (PGA, MW = 7.2×10^4 Da) were purchased from Sigma (St. Quentin Fallavier, France), and poly(ethylenimine) (PEI, MW = 7.0×10^4 Da) was obtained from Polysciences (Warrington, PA).

Tris(hydroxymethyl)aminomethane (Tris), 2-(*N*-morpholino)ethanesulfonic acid (MES), and sodium dodecyl sulfate (SDS) were also obtained from Sigma. All solutions were prepared using ultrapure water (Milli Q-plus system, Millipore) with a resistivity of 18.2 MΩ·cm. Polyelectrolyte solutions were always freshly prepared by direct dissolution of the respective adequate weights in filtered buffer solutions.

For both systems (PSS/PAH and PGA/PLL), a precursor layer of PEI was deposited on the substrate. For PEI−(PSS/PAH)$_i$ films where i corresponds to the number of layer pairs, each polyelectrolyte was dissolved in Tris-HCl buffer (0.5 mM Tris, pH 7.35) containing 0.15 M NaCl. For PEI−(PGA/PLL)$_i$ films, the buffer used for polyelectrolyte dissolution was MES-Tris (MES 25 mM, Tris 25 mM, pH 7.4) containing 0.10 M NaCl. All the final polyelectrolyte concentrations were of 5 mg/mL.

For streaming potential experiments, since the experimental device is extremely sensitive to very slight pH changes, PLL and PGA solutions were prepared in a Tris-HCl buffer (0.5 mM Tris, 0.15 M NaCl, pH 7.35) and at polyelectrolyte concentrations of 1 mg/mL.

Atomic Force Microscopy. Glass slides (Polylabo, Strasbourg, France) were used and cleaned with 10 mM SDS and 0.1 N HCl and extensively rinsed with pure water and dried under nitrogen. After this cleaning procedure, the silica surface appears to be perfectly flat (rms < 0.3 nm). A drop of the first polycation solution (PEI) was deposited over the slide and left for 15 min. Then a rinsing is performed with 1 mL of buffer solution. The polyanion is then deposited in the same manner. After deposition of i layer pairs, the film will be denoted as PEI−(PSS/PAH)$_i$ or PEI−(PGA/PLL)$_i$. Each film observed at a given stage of the construction corresponds to a totally new buildup. For all the observations, the samples were kept in the buffer solution.

Atomic force images were obtained in contact mode in buffer with the Nanoscope IIIa from Digital Instruments (Santa Barbara, CA). Cantilevers with a spring constant of 0.03 N/m and with silicon nitride tips were used (model MLCT-AUHW Park Scientific, Sunnyvale, CA). We always performed several scans over a given surface area. These scans had to produce reproducible images to ascertain that there is no sample damage induced by the tip. Deflection and height mode images are scanned simultaneously at a fixed scan rate (between 2 and 4 Hz) with a resolution of 512 × 512 pixels.

For PSS/PAH and PGA/PLL systems, rms (root-mean-square) values of samples surfaces are calculated from images covering an area of $10 \times 10\ \mu m^2$. Then a square of $5 \times 5\ \mu m^2$ is displaced on the image, and rms values at each position are calculated. Finally, we obtain a minimal and a maximal value of rms for each image.

Profilometric section analyses allow, beside rms, to precisely determine locally at the outer part of the film well or crack depths. They are achieved by cross sections of the images in the Y orientation, perpendicular to the scanning direction.

Optical Waveguide Lightmode Spectroscopy. The (PLL/PGA)$_i$ and (PSS/PAH)$_i$ film buildup process, i being the number of deposition cycles or layer pairs, was followed by OWLS. Briefly, OWLS is sensitive to the penetration depth of an evanescent wave through the film near the waveguide surface (roughly over 200 nm) and gives access to the optical properties of the film.[22,23] Details of the analysis of the optical data can be found elsewhere.[7]

The buildup of the polyelectrolyte films is performed as follows: after the buffer flow is stopped, 100 μL of the polycation solution is manually injected in the cell through the injection port. After 12−15 min (sufficient to reach a plateau), the buffer flow is restarted for 12−15 min to rinse the excess material from the cell. In the same way the alternate adsorption of polyanions and polycations was continued on the waveguide. Thus, progressively PEI−PSS, PEI−(PSS/PAH), ..., PEI−(PSS/PAH)$_i$ structures (and PEI−(PGA/PLL)$_i$) are deposited.

Streaming Potential Measurements. Streaming potential measurements were carried out in order to determine the ζ potential of the multilayers. The experiments were performed on a homemade apparatus developed by Zembala and Dejardin[24] that has been previously described.[7,25] The basic principle is to measure the pressure and the potential differences on both sides of a 530 μm radius capillary made of fused silica via two flasks containing four electrodes.

The capillary is first filled and rinsed several times with the Tris-HCl buffer and left at rest overnight for equilibration. Second, the streaming potential of the bare capillary filled with Tris-HCl buffer is measured. Then, 8 mL of the PEI solution is injected through the capillary with a syringe and left at rest for a 20 min adsorption time. The capillary is rinsed and equilibrated by injection of 100 mL of Tris-HCl buffer before the streaming potential is measured. The PGA solution is then injected through the capillary in a similar way, and streaming potential is measured by following the same procedure. PLL and PGA adsorptions are then alternately performed, and after each deposition step, the streaming potential is measured.

III. Results and Discussion

The buildup process of the films was first followed by OWLS. Figure 1 shows the typical evolution of the effective refractive index relative to the TM mode, N(TM), for the PSS/PAH (Figure 1A) and PGA/PLL systems (Figure 1B,C). Qualitatively, a similar evolution is found for N(TE), the effective refractive index relative to the TE mode. The steady increase of N(TM) as the buildup process goes on clearly indicates the alternate deposition of the polyanions and polycations. A quantitative analysis of these data requires a model for the refractive index profile of the film. We used the homogeneous and isotropic monolayer model which was shown to accurately describe polyelectrolyte multilayers.[7] Parts A and B of Figure 2 show the evolution respectively of the optical thickness d_A and the optical mass $(n_A - n_C)d_A$ of the film as a function of the number i of deposited layer pairs. As expected, both d_A and $(n_A - n_C)d_A$ increase linearly with i for the PSS/PAH system. On the other hand, a superlinear increase of both quantities is observed for the PGA/PLL system. One can also notice that thicknesses are much larger for PGA/PLL multilayers than for PSS/PAH ones. The

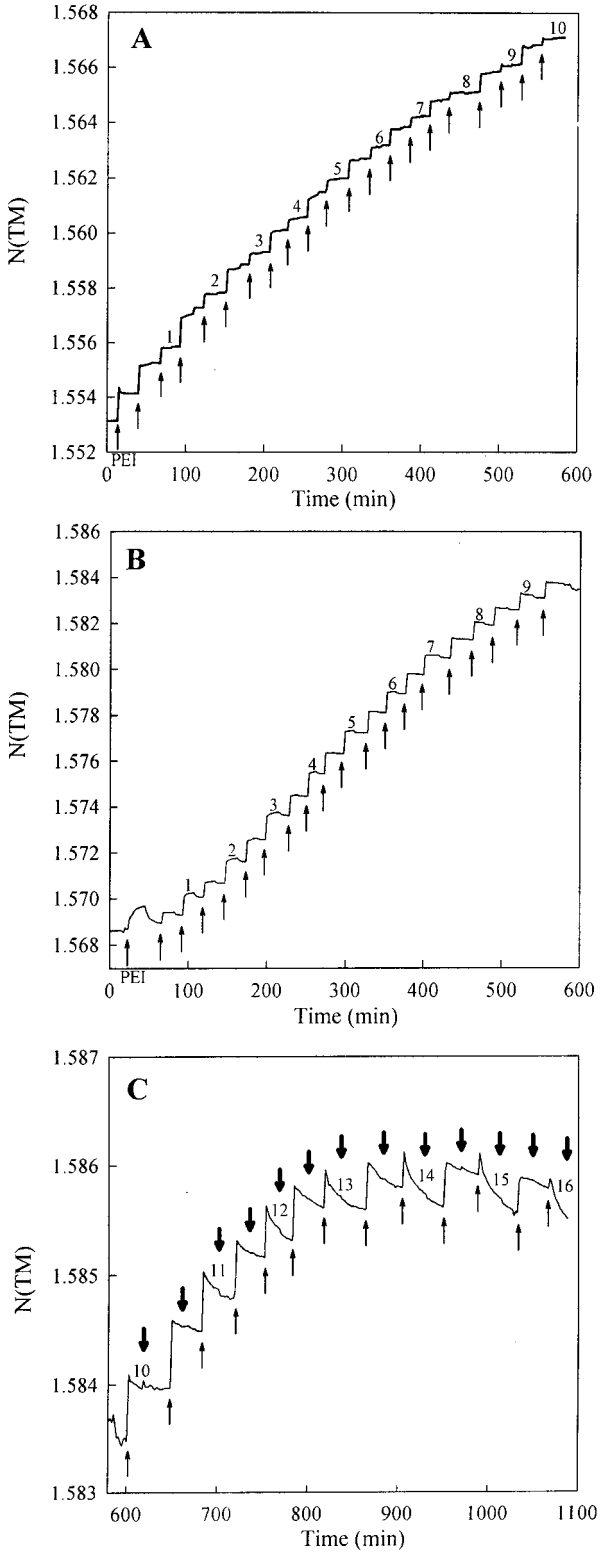

Figure 1. (A) Raw N(TM) signals obtained during PEI−(PSS/PAH)$_{10}$ multilayers buildup as measured by the OWLS technique, as a function of time. Thin long arrows indicate polyelectrolyte injection, and the numbers above the curve correspond to the achievement of the buildup of the layer pairs i (PEI−(PSS/PAH)$_i$). (B) Raw N(TM) signal obtained during the alternate deposition of PEI−(PGA/PLL)$_{10}$ multilayers as measured by the OWLS technique, as a function of time. Arrows and numbers: same meaning as for (A). (C) Same as (B) but for deposition of 11th to 16th layer pairs. For clarity of this figure, thick short arrows have been added downward and correspond to the injection of buffer for rinsing.

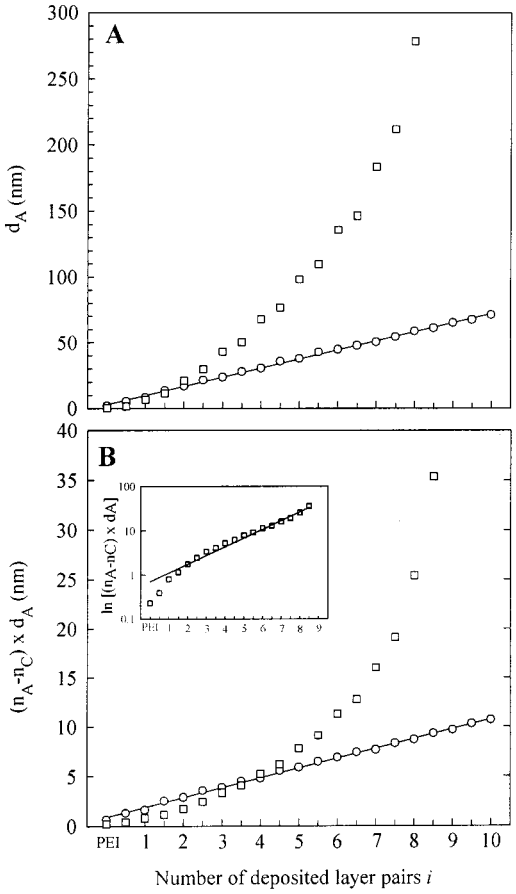

Figure 2. Evolution of the polyelectrolyte film thickness d_A (A) and optical mass $(n_A - n_C)d_A$ (B) as measured by OWLS and as a function of the numbers of added layer pairs i (PEI−(PSS/PAH)$_i$ or PEI−(PGA/PLL)$_i$): for a PEI−(PSS/PAH)$_{10}$ film (○) and for a PEI−(PGA/PLL)$_8$−PGA film (□).The inset in (B) represents the evolution of the adsorbed amount, in a logarithmic scale, noted $\ln[(n_A - n_C)d_A]$ for the PGA/PLL system as a function of the number of deposited layers. Black line is a linear regression on this logarithmic plot.

latter films had also higher refractive indices (on the order of 1.48−1.50) than the former ones, for which values in the range 1.40−1.42 were found. This indicates that the PSS/PAH films have a higher density than the PGA/PLL ones. By taking into account the stronger interaction between PSS and PAH chains compared to PGA and PLL ones, PSS being a strong polyelectrolyte and PGA and PLL being both weak polyelectrolytes, the lower refractive index of the PGA/PLL films compared to the that of PSS/PAH ones is consistent with the suggestion of Dubas and Schlenoff.[26] These authors state that strongly interacting segments cannot be easily swollen so that the thickness increment will be lower for films constituted by strong polyelectrolytes.

For the PGA/PLL system, it was no longer possible to get, out of the rough optical data, the thickness and the optical mass when more than nine layer pairs were deposited. This happens roughly when this film reaches an optical thickness of the order of 300 nm. This is due to the fact that OWLS is an optical technique based on the phase change induced in the reflected field by an evanescent wave sensing the film toward the solution. The penetration depth of this evanescent wave is of the order of 150 nm.[17] When the film thickness largely exceeds this penetration length, OWLS becomes insensitive to the film structure of the upper part, and one

can no longer determine the film thickness. In the inset of Figure 2 is represented, for the same data relative to the PGA/PLL system, the evolution of the logarithmic optical mass noted $\ln[(n_A - n_C)d_A]$ as a function of the number of deposited layers. After the deposition of the first few layers one observes, with a good approximation, a linear relationship between $\ln[(n_A - n_C)d_A]$ and i. This strongly indicates that the PGA/PLL film grows exponentially with the number of layers. After the deposition of the ninth layer pairs, the film thickness thus largely exceeds 300 nm, which is also confirmed by the fact that for larger films N(TE) and N(TM) level off (Figure 1). Such a leveling off is not observed for the PSS/PAH system (data not shown). However, one would expect that for the thick PGA/PLL films the optical signal would remain insensitive to further deposited layers, which is not the case. In contrary, N(TE) and N(TM) vary significantly after each new contact of the film as well as with PLL and PGA solutions (Figure 1C). A similar behavior has been observed for the PLL/HA system. This can only be explained by a modification of the film properties after each new deposition of PLL or PGA and after each rinsing step, leading to a change in the refractive index of the film up to the penetration zone of the evanescent wave. It must be pointed out that, although an exponential growth of the PLL/PGA films was observed in a reproducible way, the absolute values of the film thickness and optical mass could vary by a factor of 2 from one experiment to the other for a given number of deposited layers. The reasons for this large variability are not clear. However, in each case the optical data could no longer be treated quantitatively once the films reached thicknesses on the order of 300 nm, which is consistent with our previous explanation.

The structure of the films was then analyzed by in situ AFM. AFM images of a precursor PEI layer on which all the films were built reveal that the PEI is homogeneously distributed over the surface and that it forms small globules of diameters smaller than 60 nm. Their exact size is however difficult to evaluate due to size effects of the sensing tip and too low resolution. Moreover, one cannot conclude whether the globules constitute the total PEI that is deposited on the surface or whether these globules lie on a thin PEI layer that covers entirely the surface.

Parts A, B, and C of Figure 3 represent typical in situ AFM images obtained respectively after the deposition of 1, 5, and 10 PSS/PAH layer pairs on the initially deposited PEI layer. Corresponding typical profilometric sections are given in Figure 4A−C. As a general rule, no important apparent structural variations can be noticed during the different stages of the buildup process which has been investigated up to PEI−(PSS/PAH)$_{10}$. At each stage, the outer structure appears to be constituted of regularly distributed small dots with characteristic sizes ranging from 30 to 80 nm. During the film buildup the number of dots per unit area has increased slightly from PEI−(PSS/PAH)$_1$ up to PEI−(PSS/PAH)$_5$. Consequently, the evolution of the rms values during the buildup reached a plateau at around 4 nm after (PSS/PAH)$_5$. The analysis of the profilometric sections reveals that the outer surface is not structurally flat but rough with maximal height amplitudes for PEI−(PSS/PAH)$_1$ (Figure 4 A) and for PEI−(PSS/PAH)$_3$ (data not shown) of around 8 nm. The mean thickness of the PEI−(PSS/PAH)$_1$ film determined by OWLS being also

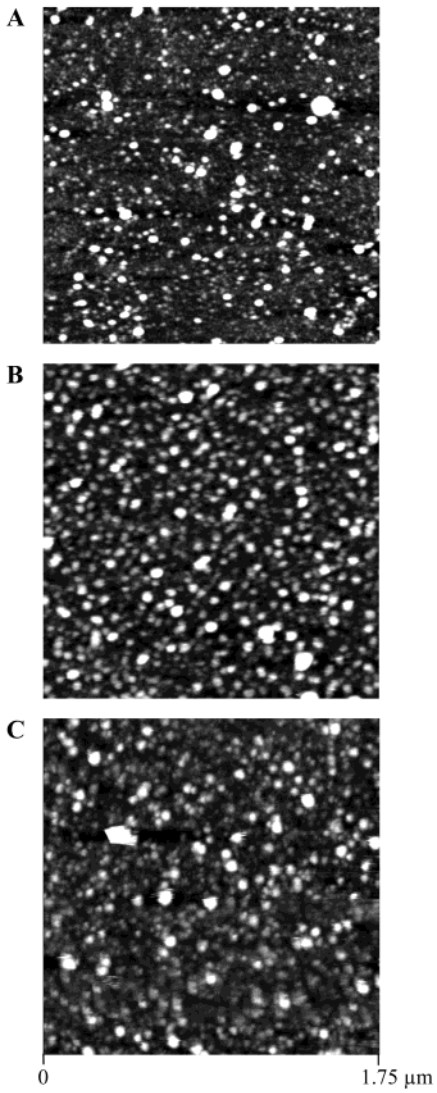

Figure 3. AFM height mode images in liquid obtained at the different steps of the alternate deposition of PSS and PAH layers on a glass substrate initially coated with a PEI layer. The polyelectrolytes PEI, PSS, and PAH were diluted in Tris-HCl buffer (0.5 mM Tris, pH 7.4) in the presence of 0.15 M NaCl and at a final concentration of 5 mg/mL. Different stages during the buildup process are visualized: (A) PEI−(PSS/PAH)$_1$, (B) PEI−(PSS/PAH)$_5$, and (C) PEI−(PSS/PAH)$_{10}$. Image dimensions are 1.75 × 1.75 μm^2, and the maximum Z ranges are 7 nm for image (A) and 15 nm for images (B) and (C).

equal to 8 nm, it cannot be excluded that part of the solid surface remains uncovered at this stage of the construction. For PEI−(PSS/PAH)$_5$ and PEI−(PSS/PAH)$_{10}$, the maximal height amplitudes are of the order of 10−12 nm (Figure 4, D and C) whereas the films thicknesses are respectively of the order 40 and 70 nm (see Figure 2A). This clearly indicates that the adsorbent surface is, at this stage, fully coated with polyelectrolytes. We did not evaluated the film thickness by scratching the film with the AFM tip because the film could only be partly removed even after several scratches. Streaming potential measurements performed on such films clearly indicate an alterning sign of the ζ potential when passing from a multilayer ending with PSS ($\zeta \approx -25$ mV) to a multilayer ending with PAH ($\zeta \approx +25$ mV) (see Ladam et al.,[25] Figure 3).

Let us now compare these results to their PGA/PLL counterparts represented in Figure 6A−C. Notice the scale difference between the images of the two systems.

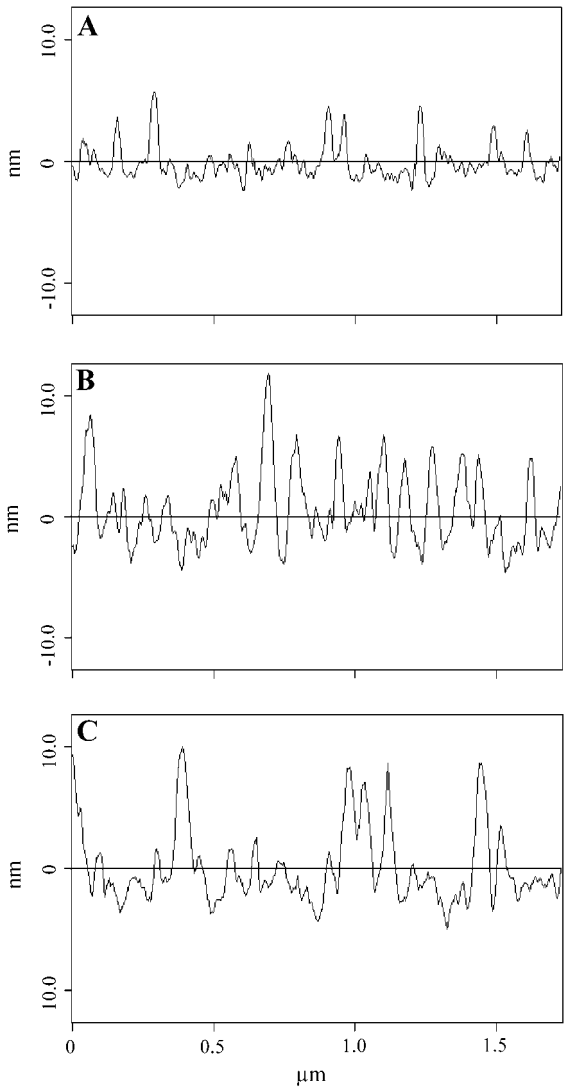

Figure 4. Profilometric sections that have been performed on the AFM images of Figure 3 and showing irregularities in height for (A) PEI−(PSS/PAH)$_1$, (B) PEI−(PSS/PAH)$_5$, and (C) PEI−(PSS/PAH)$_{10}$. The horizontal black line corresponds to the zero value in *Z* arbitrarily defined by the apparatus.

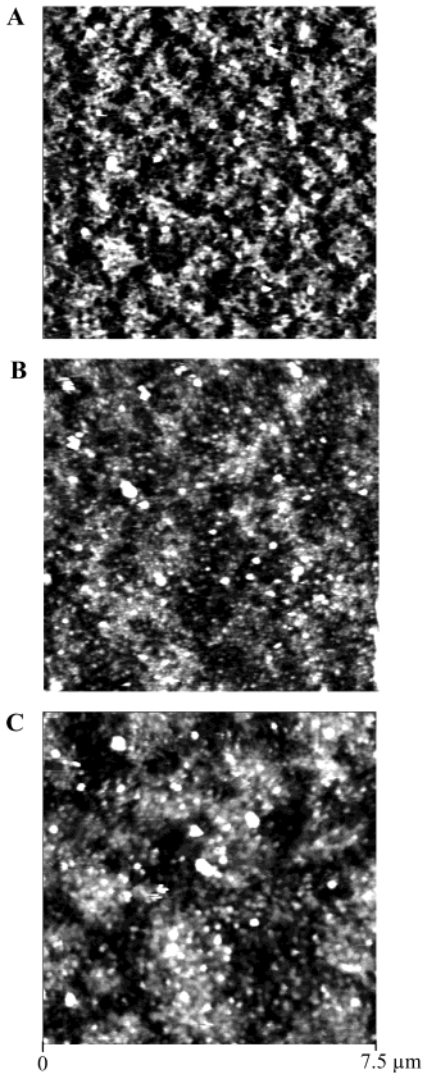

Figure 5. AFM height mode images in liquid obtained at the different steps of the alternate deposition of PGA and PLL layers on a glass substrate initially coated with a PEI layer. PEI, PGA, and PLL solutions were prepared at 5 mg/mL in MES-Tris buffer (25 mM MES, 25 mM Tris, pH 7.35) containing 0.1 M NaCl. Different stages during the buildup process are visualized: (A) PEI−(PGA/PLL)$_1$, (B) PEI−(PGA/PLL)$_5$, and (C) PEI−(PGA/PLL)$_{10}$. Images dimensions are 7.5 × 7.5 μm^2, and the maximum *Z* ranges are 20 nm for image (A) and 50 nm for images (B) and (C).

The topographies of the films of the two systems are totally different. While only small dispersed granules appeared on the (PSS/PAH)$_i$ films, the surfaces of the (PGA/PLL)$_i$ multilayers become highly granular, and the individual granules form, in addition, extended structures. The size of the grains or dots ranges between 200 and 400 nm instead of 30−80 nm for the PSS/PAH system. At a length scale of 50 × 50 μm^2 a vermiculate pattern quite similar to those observed by McAloney et al.,[12] although at a different length scale (of the order of 2−5 μm for a PEI−(PGA/PLL)$_{10}$ film and 0.2−0.5 μm for a (PDDA/PSS)$_{10}$ multilayer), clearly emerges (data not shown).

In contrast to the PSS/PAH system, we were also able to scratch the surface of the PEI−(PGA/PLL)$_i$ films with the cantilever and to measure the film thickness directly by AFM. We found respectively thicknesses of the order of 8, 20, 30, and 160 nm for PEI−(PGA/PLL)$_1$, PEI−(PGA/PLL)$_3$, PEI−(PGA/PLL)$_5$, and (PEI−PGA/PLL)$_{10}$ films. It must be noticed that each observation was performed on an independently constructed architecture. Because of the uncertainty found by OWLS in the optical thickness of the (PGA/PLL)$_i$ films, these values can be considered to be in agreement with the optical experiments. The comparison between the film thicknesses and the profilometric sections (Figure 6A−C) reveals several features. For PEI−(PGA/PLL)$_1$, irregularities of more than 13 nm in height are visible. This confirms that the silica surface on which the film was deposited is probably not fully covered with material since the mean film thickness is about 8 nm. The same observation holds for the PEI−(PGA/PLL)$_3$ film whose thickness is of the order of 20 nm and whose irregularities can be as large as the film thickness (data not shown). For thicker films (i = 5 and 10), the maximum height amplitudes of the film profile are of the order of 25 nm and are thus (much) smaller than the film thickness. The (PGA/PLL) polyelectrolyte multilayers thus cover completely the silica surface after PEI−(PGA/PLL)$_5$. Moreover, the vertical scale of the film roughness does not increase significantly during the film buildup. The larger scale inhomogeneities, i.e., the vermiculate

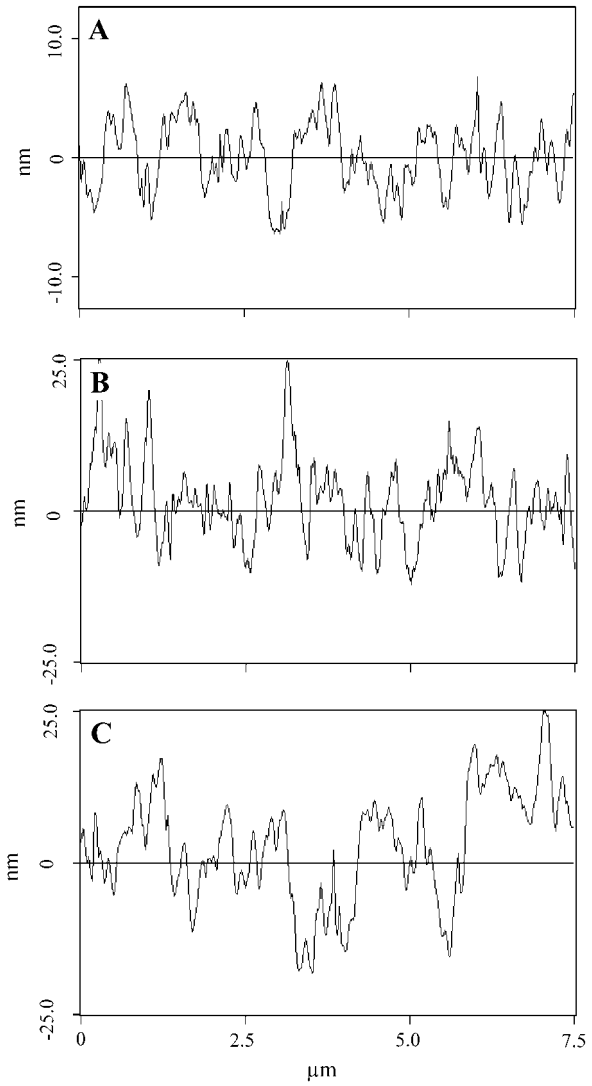

Figure 6. Profilometric sections of AFM images of Figure 5 showing irregularities in height for (A) PEI−$(PGA/PLL)_1$, (B) PEI−$(PGA/PLL)_5$, and (C) PEI−$(PGA/PLL)_{10}$. The horizontal black line corresponds to the zero value in *Z* arbitrarily defined by the apparatus.

patterns, increase in size only laterally. This result is also consistent with the observations of McAloney et al.[12] for the PDDA/PSS system. Correlatively, one finds that the rms values first increase with the number of deposited layers before reaching a plateau of about 10 nm after PEI−$(PGA/PLL)_5$. For the PGA/PLL system, the exponential growth can thus not be the consequence of an increase of the film roughness during the buildup as suggested in the literature for other systems.[10] Further evidence of this is provided by ζ potential measurements on this system. We found that, despite the exponential growth regime, the ζ potential of the film does not vary during the buildup but evolves between two constant values respectively of +80 mV for the PLL and −60 mV for the PGA ending films (Figure 7). This shows that the charge excess that appears at the outermost layer remains constant, and it is reasonable to assume that this charge excess is mainly present in the rough part of the film.

We propose the following model to explain both the exponential growth and the AFM observations (Figure 8): consider first a $(PGA/PLL)_i$ multilayer architecture. In addition to the PLL chains that form the outer layer

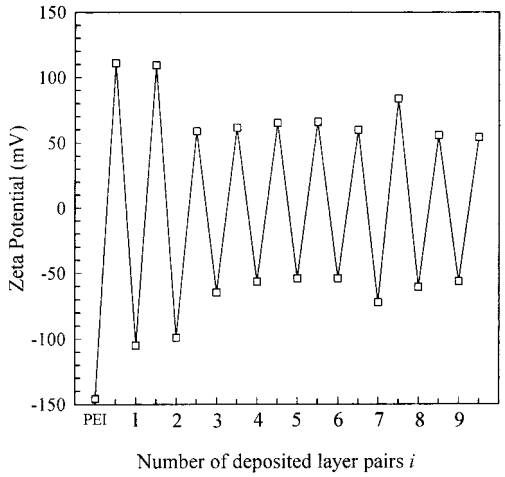

Figure 7. Evolution of the ζ potential (mV) during the alternate deposition of PLL and PGA on the top of a PEI layer as a function of the layer pairs *i* added. PLL and PGA were prepared at 1 mg/mL in a 0.5 mM Tris-HCl buffer (pH = 7.4) containing 0.1 M NaCl. The line has no physical meaning and was added for the clarity of the figure. Each point represents the mean value of three successive measurements. Standard deviations are so small that they are not visible on the graph.

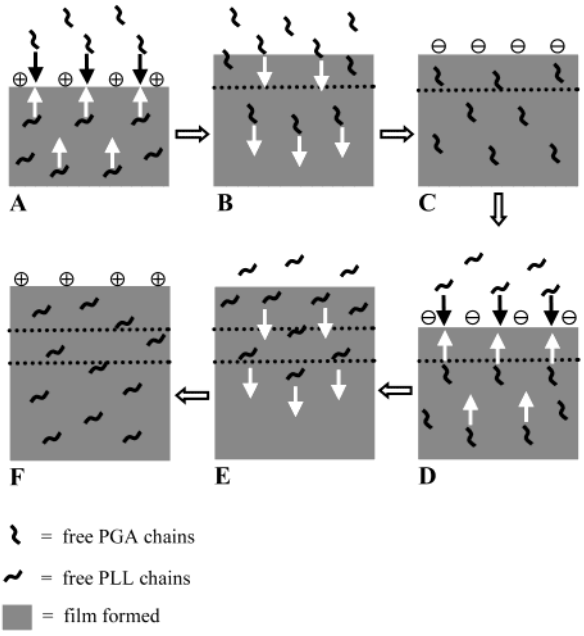

Figure 8. Schematic drawing of the buildup mechanism of PGA/PLL multilayers. For details, see the main text. (A) Beginning of the contact between a $(PGA/PLL)_i$ multilayer with a PGA solution. (B) Diffusion of PGA chains into the film once all the mobile PLL chains have diffuse out of it. (C) End of step B resulting in a negative charge overcompensation on the film. (D) Beginning of the contact between a $(PGA/PLL)_i$−PGA multilayer with a PLL solution. (E) Diffusion of PLL chains into the film once all the mobile PGA chains have diffuse out of it. (F) End of step E resulting in a positive charge overcompensation of the $(PGA/PLL)_{i+1}$ film.

are responsible for the charge overcompensation, we will assume that the film contains two kinds of PLL chains: chains that are strongly involved in interaction with PGA and which constitutes the network of the multilayer and chains that are weakly bond to the polyelectrolyte structure forming the film. These mobile chains can diffuse within the film structure. The excess charge provided by these chains must be compensated by the presence of small counterions. When such a film is

brought in contact with a PGA solution, the PGA chains will first strongly interact with the PLL chains forming the outermost layer (Figure 8A). On the other hand, the PLL chains that are mobile in the interior of the film structure slowly diffuse out of it. As soon as the PLL chains reach the film/solution interface, they react with PGA chains from the solution to form PLL/PGA complexes. These complexes are usually neutral. The film/solution interface thus acts as a perfect sink for the mobile PLL chains in the film, and this constitutes one of the major driving force for the "out" diffusion. The diffusing PLL being only slightly bond to the film, these complexes are only weakly anchored on the multilayer. They are thus quite mobile over the film and can interact one with each other to form larger entities as they are seen in solution when two polyelectrolytes of opposite charge are mixed. These entities, made of PLL/PGA complexes, could be the structures seen on the AFM images that form the larger scale pattern. These structures must be highly swollen. When most of the mobile PLL chains have diffused to the surface of the film, PGA chains start to diffuse into the film (Figure 8B), and a charge overcompensation on the film starts again to build up due to the presence of the excess of PGA chains in solution (Figure 8C). Most of these PGA chains that have diffused in the interior of the film are free chains. Because PGA/PLL are dynamic complexes, some of the free chains can establish interactions with PLL chains inside of the film in a kind of exchange mechanism. These will become weakly bond PGA chains. When the PGA solution is rinsed with a polyelectrolyte-free aqueous solution, most of the free PGA chains will diffuse out of the film, but there remain weakly bond PGA chains within the film. These "in" and "out" diffusion processes accompanied by a kind of exchange mechanism can lead to continuous film restructurations, inducing changes in the refractive index of the whole film. Such a process must occur in order to explain the cyclic changes in OWLS signals when the film become very thick (Figure 1C). The process can now start again, PLL playing the role of PGA (Figure 8D,F), and vice versa. After each diffusion process "into" the film, the number of weakly bond chains must, in first approximation, be proportional to the film thickness. Moreover, the mass of PGA/PLL complexes that form above the film must be proportional to the number of weakly bond polyelectrolytes that diffuse out of the film. This should lead to an exponential growth of the deposited mass of polyelectrolytes and thus also of the film thickness.

The linear evolution of both mass and thickness increments for the PSS/PAH system could be due to a denser structure of these films compared to the PGA/PLL system, avoiding important polyelectrolyte diffusion inside the film. The fact that the refractive index of the PSS/PAH films is higher than that of the PGA/PLL films ($\sim$1.50 for PSS/PAH and $\sim$1.42) and that their thickness and roughness are lower strengthen this hypothesis. It should be noticed that different ionic strength or pH conditions could lead the PSS/PAH system to follow a superlinear growth regime and the PGA/PLL system to follow a linear growth regime. However, we have not found, up to now, such conditions for these two systems.

Finally, one can also notice that the PGA/PLL system is, in some respect, particular because both polypeptides can interact one with each other not only through electrostatic interactions but also through hydrogen bonds[27] and can form α-helix and β-sheet structures within the films.[28] The formation of such secondary structures can lead to film inhomogeneities at a nanometer length scale. This could favor the "in" and "out" diffusion of the polypeptides in the film. These interactions can eventually also be at the origin of the film restructuration after each "in" and "out" diffusion process. Moreover, the film structure may depend somewhat on the buildup conditions of the assembled film.

One must nevertheless keep in mind that a similar "in" and "out" diffusion process seems also to take place for the system poly-L-lysine/hyaluronic acid (PLL/HA) which growth also in a superlinear way. The proposed mechanism for such a superlinear growth regime based on polyelectrolyte diffusion seems thus not to be particular to the (PGA/PLL) system but represents a second general way, besides the mechanism based on the increase of roughness, for a system to grow superlinearly.

IV. Conclusion

$(PGA/PLL)_i$ polyelectrolyte multilayers have been structurally characterized and compared to the more widely studied $(PSS/PAH)_i$ films. As determined by optical waveguide lightmode spectroscopy, the PGA/PLL system exhibits an exponential growth regime in contrary to the PSS/PAH system whose growth regime is linear in our buildup conditions. We found that, despite this exponential growth, the ζ potential of the $(PGA/PLL)_i$ films alternates between two almost constant values of opposite sign during the whole film construction. Careful in situ observations of the multilayers buildup process have been performed by means of AFM imaging up to 10 layer pairs. The structure of the $(PSS/PAH)_i$ films appears to be constituted by small grains that remain almost the same over the whole buildup process. On the other hand, the structure of the $(PGA/PLL)_i$ films is highly granular. These granules form extended structures that generate a vermiculate pattern at the micron scale. The roughness of these films remains almost constant during their buildup after the first five layer pairs have been deposited. This suggests that for the PGA/PLL system the nonlinear growth cannot be due to an increase of the film roughness during buildup as suggested in the literature for other systems.[10] We finally propose a mechanism based on polyelectrolyte diffusion "in" and "out" of the core of the polyelectrolyte multilayers to explain the exponential growth observed for the PGA/PLL system. Such a mechanism was already suspected for the $(PLL/HA)_i$ films[17] exhibiting an exponential growth regime.

Acknowledgment. This work was supported by CNRS and INSERM through the program "Ingénierie tissulaire", by the European Community through the SIMI program, and by the Ministère de la Recherche through the ACI "Technologies pour la Santé" and ACI "Surfaces, interfaces et conception de nouveaux matériaux".

References and Notes

(1) Decher, G.; Hong, J. D.; Schmitt, J. *Thin Solid Films* **1992**, *210/211*, 831−835.
(2) Decher, G. *Science* **1997**, *277*, 1232−1237.
(3) Schlenoff, J.; Ly, H.; Li, M. *J. Am. Chem. Soc.* **1998**, *120*, 7626−7634.

(4) Decher, G. In *Comprehensive Supramolecular Chemistry: Templating, Self-Assembly and Self-Organization*; Sauvage, J. P., Hosseini, M. W., Eds.; Pergamon Press: Oxford, 1996; Vol. 9, pp 507−528.
(5) Caruso, F.; Niikura, K.; Furlong, D. N.; Okahata, Y. *Langmuir* **1997**, *13*, 3422−3426.
(6) Ramsden, J. J.; Lvov, Y. M.; Decher, G. *Thin Solid Films* **1995**, *254*, 246−251.
(7) Picart, C.; Ladam, G.; Senger, B.; Voegel, J.-C.; Schaaf, P.; Cuisinier, F. J. G.; Gergely, C. *J. Chem. Phys.* **2001**, *115*, 1086−1094.
(8) Yoo, D.; Shiratori, S. S.; Rubner, M. F. *Macromolecules* **1998**, *31*, 4309−4318.
(9) Lösche, M.; Schmitt, J.; Decher, G.; Bouwman, W. G.; Kjaer, K. *Macromolecules* **1998**, *31*, 8893−8906.
(10) Ruths, J.; Essler, F.; Decher, G.; Riegler, H. *Langmuir* **2000**, *16*, 8871−8878.
(11) Kim, D. K.; Han, S. W.; Kim, C. H.; Hong, J. D.; Kim, K. *Thin Solid Films* **1999**, *350*, 153−160.
(12) McAloney, R. A.; Sinyor, M.; Dudnik, V.; Goh, M. C. *Langmuir*, in press.
(13) Advincula, R.; Aust, E.; Meyer, W.; Knoll, W. *Langmuir* **1996**, *12*, 3536−3540.
(14) Elbert, D. L.; Herbert, C. B.; Hubbell, J. A. *Langmuir* **1999**, *15*, 5355−5362.
(15) Pardo-Yissar, V.; Katz, E.; Lioubashevski, O.; Willner, I. *Langmuir* **2001**, *17*, 1110−1118.
(16) Cheng, Y.; Corn, R. M. *J. Phys. Chem. B* **1999**, *103*, 8726−8731.
(17) Picart, C.; Lavalle, P.; Hubert, P.; Cuisinier, F. J. G.; Decher, G.; Schaaf, P.; Voegel, J. C. *Langmuir* **2001**, *17*, 7414−7424.
(18) Sukhorukov, G. B.; Schmitt, J.; Decher, G. *Ber. Bunsen-Ges. Phys. Chem.* **1996**, *100*, 948−953.
(19) Mendelsohn, J. D.; Barrett, C. J.; Chan, V. V.; Pal, A. J.; Mayes, A. M.; Rubner, M. F. *Langmuir* **2000**, *16*, 5017−5023.
(20) Fery, A.; Schöler, B.; Cassagneau, T.; Caruso, F. *Langmuir* **2001**, *17*, 3779−3783.
(21) Lvov, Y.; Ariga, K.; Onda, M.; Ichinose, I.; Kunitake, T. *Colloids Surf. A* **1999**, *146*, 337−346.
(22) Tiefenthaler, K.; Lukosz, W. *J. Opt. Soc. Am. B: Opt. Phys.* **1989**, *6*, 209−220.
(23) Ramsden, J. J. *J. Mol. Recogn.* **1997**, *10*, 109−120.
(24) Zembala, M.; Dejardin, P. *Colloids Surf. B* **1994**, *3*, 119−129.
(25) Ladam, G.; Schaad, P.; Voegel, J. C.; Schaaf, P.; Decher, G.; Cuisinier, F. *Langmuir* **2000**, *16*, 1249−1255.
(26) Dubas, S. T.; Schlenoff, J. B. *Macromolecules* **2001**, *34*, 3736−3740.
(27) Sukhishvili, S. A.; Granick, S. *Macromolecules* **2002**, *35*, 301−310.
(28) Cooper, T. M.; Campbell, A. L.; Noffsinger, C.; Gunther-Greer, J.; Crane, R. L.; Adams, W. *Mater. Res. Soc. Symp. Proc.* **1994**, *351*, 239−244.

MA0119833